

## Freestanding graphene writing on a silicon carbide wafer

E.H. Kim<sup>a,1</sup>, J.H. Park<sup>a,1</sup>, I.B. Khadk<sup>a,1</sup>, J. Son<sup>a</sup>, H.W. Kim<sup>a</sup>, D.H. Lee<sup>a</sup>, B.J. Kim<sup>a</sup>, D.I. Sung<sup>b</sup>, S. H. Woo<sup>c</sup>, G.Y. Yeom<sup>b,d</sup>, S.H. Park<sup>a,d</sup>, J.R. Ahn<sup>a,d,\*</sup>

<sup>a</sup> Department of Physics, Sungkyunkwan University, Suwon 16419, Republic of Korea

<sup>b</sup> School of Advanced Materials Science and Engineering, Sungkyunkwan University, Suwon 16419, Republic of Korea

<sup>c</sup> College of Pharmacy, Chungnam National University, Daejeon 305–764, South Korea

<sup>d</sup> Sungkyunkwan Advanced Institute of Nanotechnology (SAINT), Sungkyunkwan University, Suwon 16419, Republic of Korea

### ARTICLE INFO

#### Keywords:

Freestanding graphene

Graphene

Raman spectroscopy

### ABSTRACT

Freestanding graphene on a trench has been fabricated extensively using a transfer process of chemical vapor deposition grown graphene. Here, we demonstrate that freestanding graphene can be grown directly on a trench without a transfer process. A shallow trench was made on a 6H-SiC(0001) wafer using a focused ion beam lithography. The shallow trench was heated to a high temperature under Ar atmosphere. The heat treatment made the shallow trench become deeper and wider. Subsequently, epitaxial graphene was floating on the trench, resulting in freestanding graphene, where underlying bulk SiC was self-etched after the growth of epitaxial graphene. The freestanding graphene on a trench was characterized using Raman spectroscopy and atomic force microscopy. Such freestanding graphene writing can be applied to semiconductor fabrication process of freestanding graphene devices without a transfer process.

### 1. Introduction

The study of freestanding graphene is considered to be a valuable research topic in terms of both fundamental physical properties and its application to devices based on it [1–4]. Numerous researches on fundamental properties have been reported, including an ultra-high electron mobility in suspended graphene [5]. The mechanical and electrical properties of freestanding graphene were studied using freestanding graphene on a trench or a hole substrate [5–7]. Especially, as a graphene membrane, the freestanding graphene can be applied to microelectromechanical system (MEMS) based sensors, biological membranes, and molecular filtration materials [2,8,9]. The freestanding graphene on a hole substrate was usually obtained by using exfoliation method from graphite, and it was used to measure its mechanical properties [10]. In addition, studies have been conducted to observe the quasi-freestanding behavior of graphene by intercalating various atoms (or molecules) between the substrate and the graphene layer [11,12]. In terms of application, chemical vapor deposition (CVD) grown graphene or graphene oxide sheets were transferred onto a hole or a trench to fabricate MEMS and optical devices or membranes [13–16]. Graphene oxide sheets transferred on a hole substrate were used for selective gas

transport [17,18]. Nano pored CVD grown graphene on a hole substrate could be used for DNA sequencing [19–21]. For MEMS as stochastic-frequency oscillators, transferred CVD graphene on a hole substrate was widely used [22,23]. Recently, graphene nano-membrane arrays was fabricated without a transfer process, where graphene was grown on a Cu film deposited on a hole substrate and subsequently the Cu film was wet-etched [24]. According to previous studies, transfer and/or wet-etching process is required to fabricate freestanding graphene that is difficult to apply to semiconductor device fabrication procedure [7,25]. Therefore, it has been highly recommended to fabricate such freestanding graphene on a trench or a hole substrate without both transfer and wet-etching process and with minimizing number of processes.

### 2. Results and discussion

Here, we demonstrate that freestanding graphene can be fabricated on a trench without a transfer process on a silicon carbide (SiC) wafer, Si-terminated surface of 6H-SiC(0001). Furthermore, the fabrication of freestanding graphene on a trench consist of simple two-step process, as show in Fig. 1. First, a shallow trench structure were made on a 6H-SiC

\* Corresponding author. Department of Physics, Sungkyunkwan University, Suwon 16419, Republic of Korea  
E-mail address: [jrahn@skku.edu](mailto:jrahn@skku.edu) (J.R. Ahn).

<sup>1</sup> E. H. Kim, J. H. Park and I. B. Khadk contributed equally to the entire work.

(0001) wafer using focused ion beam (FIB) lithography (see Fig. 1(a)). The trench structured SiC wafer was heated in 180 torr of argon gas at 1800 °C for 7 min. Epitaxial graphene began to be created on the heated SiC surface. Then, the graphene was grown along the trench, as shown in Fig. 1(b). Interestingly, with further heating, the bulk SiC around the trench was self-etched and the graphene on the trench exhibits freestanding behavior (Fig. 1(c)). The self-etching occurred due to the sublimation of Si atoms within trench. The Si atoms evaporated out and C atoms contributed to forming freestanding graphene as shown in the schematic illustration Fig. 1(d). The bulk SiC was self-etched by Si-sublimation in the original trench at high temperature. As a result of self-etching, the shallow trench became deeper and wider. Consequently, epitaxial graphene that grew along the shape of the trench became a freestanding graphene due to the expansion of the shallow trench, as shown in Fig. 1(c). This directly grown freestanding graphene has a structural similarity of the graphene transferred over the trench from graphite or CVD grown graphene. However, this freestanding graphene does not require any transfer or wet-etching process because bulk SiC could be self-etched during the growth of the graphene.

Fig. 2 shows the freestanding graphene grown on various trenches. The shallow trenches with a 40  $\mu\text{m}$  length and a 250 nm depth were fabricated on a 6H-SiC(0001) wafer using FIB lithography and their widths ranged from 1 to 2  $\mu\text{m}$ , where Fig. 2(a) shows atomic force microscopy (AFM) images of the shallow trenches. The trench structured SiC wafer was heated to 1800 °C in 180 torr Ar atmosphere for 7 min. Fig. 2(b) shows a Raman map image of epitaxial graphene grown on the shallow trenches, in terms of the ratio of the 2D and G peak intensity ( $I_{2D}/I_G$ ) of a Raman spectrum. Here, the two representative Raman peaks of graphene, called G ( $\sim 1580\text{ cm}^{-1}$ ) and 2D ( $\sim 2700\text{ cm}^{-1}$ ), originate from the breathing modes of  $\text{sp}^2$  carbon atoms and two phonons with opposing momentum in the highest optical branch near the K point of the Brillouin zone of graphene [26]. The Raman map image suggests that the epitaxial graphene was grown on the overall surface area of the SiC wafer. However, the different intensity ratio value between the inside and outside of the trench shows that the characteristics of epitaxial graphene inside trench is quite different from outside trench. The  $I_{2D}/I_G$  intensity ratio value was above 1 on the inside of the trench region and below 1 on the outside of the trench region, respectively. To understand the characteristics of the epitaxial graphene, we measured the Raman spectra on the inside and outside of the trench, as shown in Fig. 2(c), where the measuring positions are indicated in Fig. 2(b). The Raman spectra obtained at the region I (inside of the trench) and II (outside of the trench) show entirely different result. The Raman spectrum at the region II is typical one of epitaxial graphene grown on SiC

substrate, where the Raman spectrum has characteristics of both graphene and bulk SiC. In contrast to the Raman spectrum at the region II, the Raman spectrum at the region I shows only characteristics of graphene. There is a finite intensity at the position of the G peak in the Raman spectrum of bulk SiC so that the intensity ratio can be below 1. When graphene is located on bulk SiC [27,28]. Furthermore, the intensity ratio suggests that the epitaxial graphene inside the trench has characteristics of bilayer graphene. The different Raman spectra suggest that bulk SiC inside trench is removed during or after the growth of epitaxial graphene. In other words, the Raman spectra show that epitaxial graphene outside the trench is located on bulk SiC and is floating from bulk SiC on the inside of the trench. For the understanding of the temperature dependence of the freestanding graphene growth, we measured Raman spectra with increasing a heating temperature up to 1900 °C, as shown in Fig. 2(d). The Raman spectra were measured on the trench after the growth of graphene that were produced with the same heating time and Ar pressure at each heating temperature, 7 min and 180 torr, respectively. The typical Raman spectrum of bulk SiC have Raman shifts between 1000 and 2000  $\text{cm}^{-1}$  (see the Raman spectrum at the bottom of Fig. 2(d)). With increasing the heating temperature, the Raman spectrum of bulk SiC fade away while the Raman spectrum of graphene grow gradually. In particular, when the heating temperature is above 1800 °C, the Raman spectrum of bulk SiC almost disappear. The temperature dependence suggests that the freestanding graphene can be synthesized at a heating temperature above 1800 °C. The blue shifts of the Raman spectra at high heating temperatures can be explained in terms of the compressive strain of epitaxial graphene grown on SiC [16, 29]. The 2D peak becomes sharper and the intensity ratio  $I_{2D}/I_G$  increases with raising the heating temperature above 1800 °C. In contrast to the freestanding graphene, when epitaxial graphene is located on bulk SiC, the 2D peak becomes broader and the intensity ratio  $I_{2D}/I_G$  decreases with raising the heating temperature or time [27,30]. The Raman spectra suggest that the characteristics of freestanding graphene become similar to that of single-layer graphene with increasing heating temperature above 1800 °C. Moreover, the full width at half-maximum (FWHM) of the Raman 2D peak is correlated with hall carrier mobility [31]. Narrower FWHM exhibit higher room temperature mobility. With narrower 2D peak FWHM from 68 to 35  $\text{cm}^{-1}$  of freestanding graphene shows a room temperature hall mobility of the freestanding graphene is increased over 3000  $\text{cm}^2/\text{Vs}$ [31]. In a recently published article, freestanding three-dimensional (3D) graphene was reported to be grown on a 3D SiC structure [4]. According to the article, bulk SiC was suggested to be self-etched during or after the growth of freestanding graphene at a similar high temperature to that used for this direct growth of

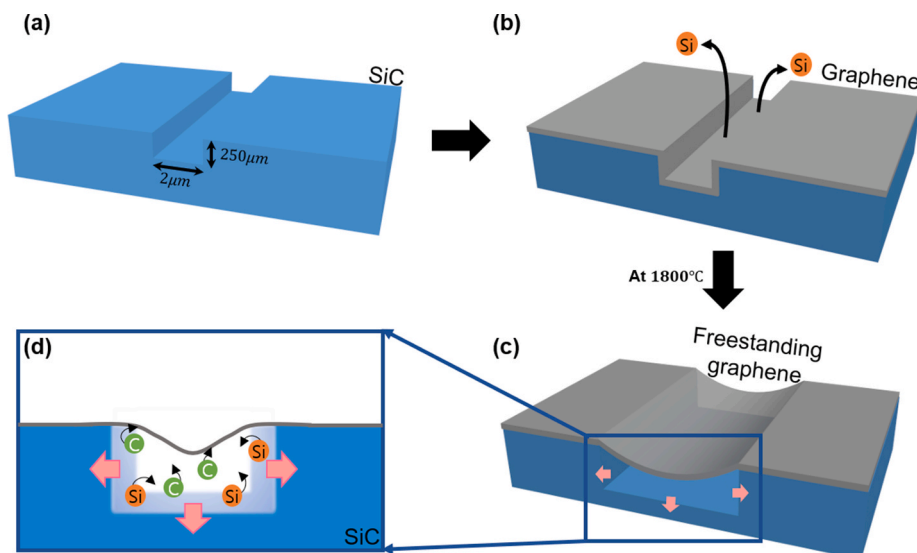
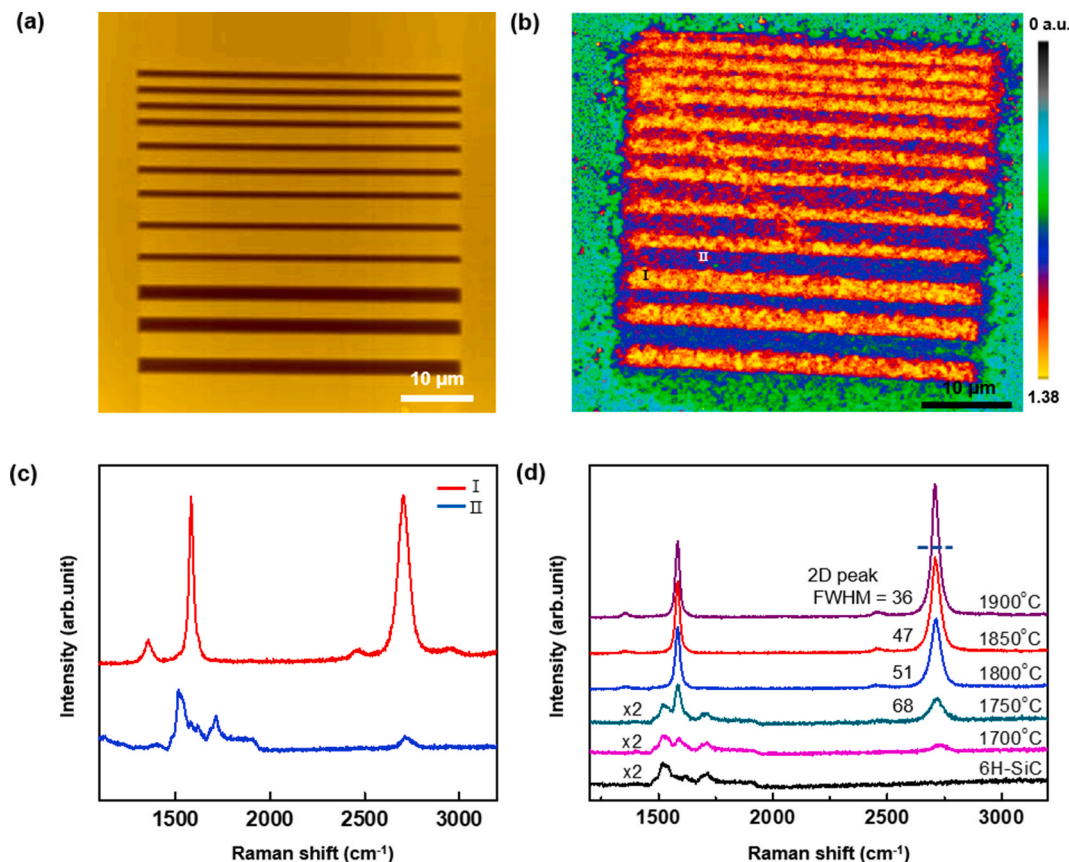


Fig. 1. (Color online) A schematic drawing of the direct growth of a designed freestanding graphene on a SiC wafer. (a) A trench on a SiC wafer. (b) The growth of graphene on the SiC trench at a high temperature of 1800 °C. (c) The graphene grown on the trench becomes freestanding after the trench is etched further at a high temperature of 1800 °C and becomes wider and deeper. (d) The mechanism of the self-etching of the SiC trench in (c). The trench is etched at a high temperature by the Si and C atoms evaporated from the SiC trench. (For interpretation of the references to color in this figure legend, the reader is referred to the Web version of this article.)



**Fig. 2.** (Color online) (a) AFM images of trenches on SiC after FIB lithography. (b) Raman mapping of the ratio of the 2D and G peak intensity ( $I_{2D}/I_G$ ) after graphene growth. (c) Raman spectra of the region I (inside trench) and II (outside trench). (d) The Raman spectra of graphene on trench of SiC measured with increasing heating temperature. (For interpretation of the references to color in this figure legend, the reader is referred to the Web version of this article.)

freestanding graphene on a trench. The self-etching can happen because Si atoms evaporated from bulk SiC are trapped temporarily between graphene and bulk SiC and etch Si and C atoms of bulk SiC. Furthermore, 3D SiC structures contain more step edges than flat SiC structures and the evaporation rate of Si atoms is much activated at step edges, compared to terraces [32–34]. Similar to the result of 3D structure, the trench also has high density of step edges so that it can be explained by the self-etching phenomenon. In contrast to the freestanding 3D graphene grown on a 3D SiC structure, freestanding two-dimensional graphene was grown on the trench. This result suggests that a convex SiC structure can be used to make freestanding 3D graphene while a concave SiC structure can be used as a platform for the fabricating freestanding 2D graphene.

As shown in Fig. 3, in order to understand the growth mechanism of the freestanding graphene, the geometrical change of the SiC trench before and after the growth of freestanding graphene was observed. Fig. 3(a) shows the AFM image of the SiC trench before the growth of freestanding graphene. The depth and width of the SiC trench were 250 and 2  $\mu\text{m}$ , respectively, as shown in the line profile of the AFM image (Fig. 3(b)). After the growth of freestanding graphene, freestanding graphene covered the SiC trench and the area was flattened, as shown in Fig. 3(c). The line profile of the AFM image (Fig. 3(d)) shows more clearly that the freestanding graphene (blue solid line) is flat in comparison to the SiC trench (red dotted line) before the growth of freestanding graphene. To observe the geometrical change of the SiC trench after the growth of freestanding graphene, freestanding graphene was removed using oxygen plasma and the SiC trench was observed using AFM. Fig. 3(e) shows that the SiC trench still exists after the growth of freestanding graphene. The line profile of the AFM image (Fig. 3(f)) provides clues of the growth mechanism of the freestanding graphene.

The SiC trench (green solid line) after the growth of freestanding graphene became deeper and wider in comparison to that (red dotted line) before the growth of freestanding graphene. This suggests that the graphene grown on the SiC trench became freestanding because of the further etching of the SiC trench, as described in Fig. 1.

The direct growth of freestanding epitaxial graphene was also studied on different types of concave structures, as shown in Fig. 4. The ring structures were made using FIB lithography. As shown in the optical image in Fig. 4(a), the ring size was 2.0, 0.5, and 0.2  $\mu\text{m}$ , respectively. A SiC wafer with the ring structures was heated at 1800  $^\circ\text{C}$  for 7 min in Ar atmosphere 180 torr. Fig. 4(b) shows an optical image after the growth of graphene. We obtained Raman spectral images on the defects, where the brightness is proportional to the intensity of 2D peak ( $I_{2D}$ ), as shown in Fig. 4(c)–(e). Two different regions were observed on each image. The clear difference in brightness is similar to that in Fig. 2(b). As described above, the difference in brightness originates from the self-etching of bulk SiC underlying epitaxial graphene. The rings with 0.5 and 0.2  $\mu\text{m}$  diameters were widened, resulting in freestanding graphene on a ring (see Fig. 4(d) and (e)). The 0.5 and 0.2  $\mu\text{m}$  diameters of the rings were widened up to 2 and 1  $\mu\text{m}$ , respectively, as shown in Fig. 4(d) and (e), where the insides of the rings look dark in the optical image in Fig. 4(b). In comparison to the rings, freestanding graphene grown on the ring with a 2.0  $\mu\text{m}$  diameter is located on a circular trench (see Fig. 4(c)). The circular trench is more clearly observable in the optical image in Fig. 4(b), corresponding to a dark ring in the image. When a heating time increases, the bottom of the ring is expected to be self-etched fully and subsequently the circular trench could be transformed into a hole shape. The difference in the shape of freestanding graphene suggests that when the area of the bottom of the ring is large enough, only the edge of the bottom is self-etched because the central region of the bottom becomes

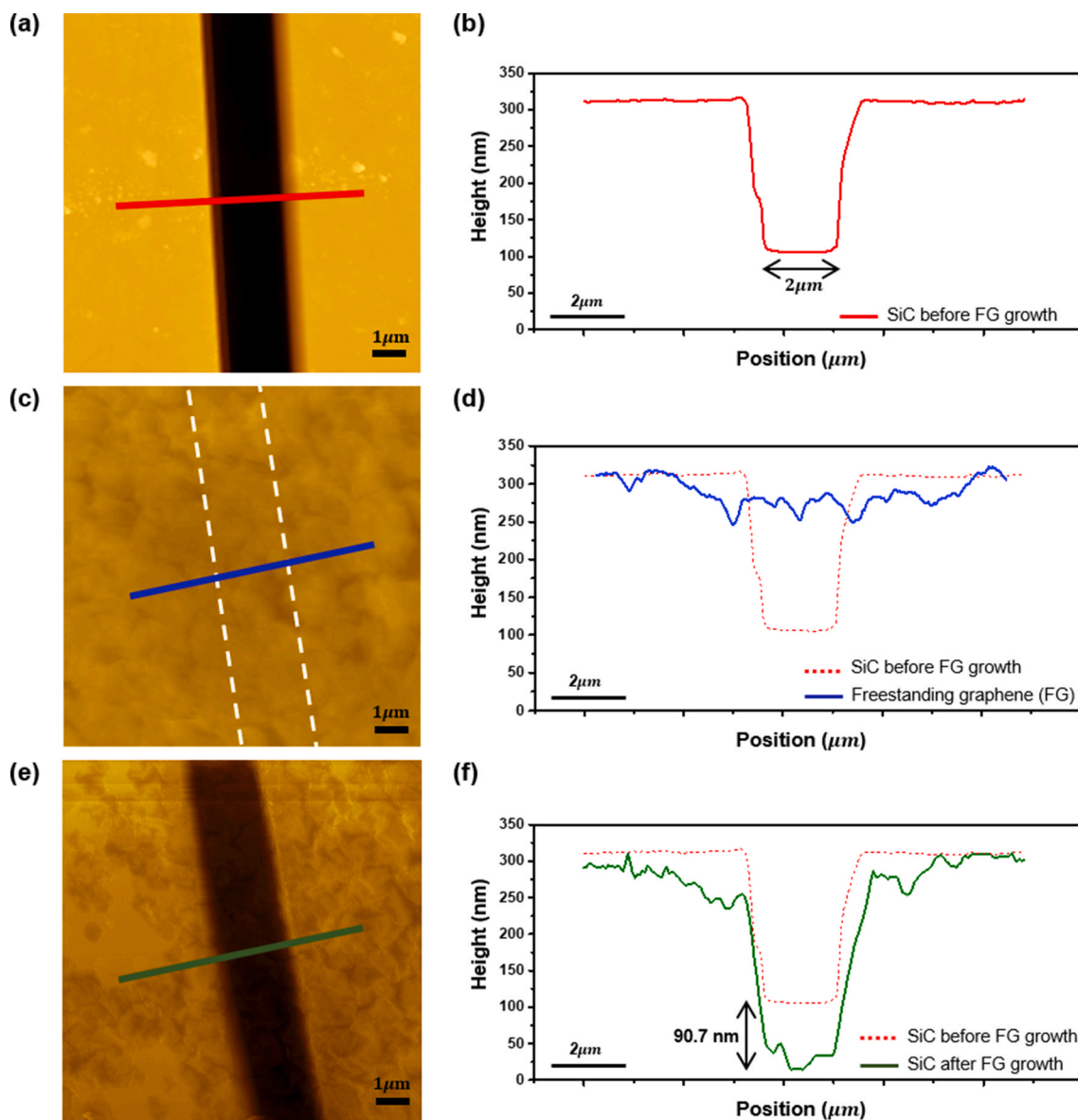


**Fig. 3.** (Color online) (a) An AFM image of a SiC trench and (b) a line profile (red solid line) across the SiC trench before the growth of freestanding graphene (FG). The line profile in (b) was measured along the red line in (a). (c) An AFM image of freestanding graphene and (d) a line profile (blue solid line) across the trench after the growth of freestanding graphene. The red dotted line in (d) is the line profile of the SiC trench before the growth of freestanding graphene. The white dotted line in (c) is the position of the SiC trench. (e) An AFM image of the SiC trench and (f) a line profile (green solid line) across the SiC trench after etching the freestanding graphene. (For interpretation of the references to color in this figure legend, the reader is referred to the Web version of this article.)

similar to a flat region. The dependence of self-etching on the size of the defective region also suggests that the self-etching is much activated at the edges and side walls of a defective region.

### 3. Conclusions

2D freestanding epitaxial graphene was directly grown on a Si-face 6H-SiC(0001) wafer using artificial concave structure fabricated by FIB lithography. The concave structures such as a trench and a hole were fabricated on a SiC wafer. High temperature heat treatments made the 2D freestanding epitaxial graphene grow on the concave structures, where the concave structures were widened and deepened. Subsequently, the epitaxial graphene was floating from the concave structures. In addition to the rectangular shape, we can construct various concave structure with the desired shape or letter, which can be transformed simply into freestanding graphene. Up to date, this method is the simplest and interesting way to fabricate 2D freestanding graphene on

concave structures. In addition, since this method does not require any transfer or wet-etching process, it is expected to be applicable to graphene-based device fabrication process.

### 4. Methods

**Sample preparation:** Concave structures were fabricated on a 6H-SiC wafer (CREE) using focused ion beam (FIB). Freestanding graphene were grown using thermal heating. Samples were heated at 1800 °C under 180 torr of argon gas (99.999% purity and 900 SCCM) for 7 min for the growth of freestanding graphene.

**Sample characterization:** Raman measurements were performed using a WITTEC Raman microscope and a WITTEC confocal microscope using a 532 nm laser and a 600/1800 groove grating. Raman maps were acquired using a laser with an output power of 1 mW and a spatial resolution of 600 nm. AFM measurements were performed using a HITACHI atomic force microscope with a contact mode. Topography

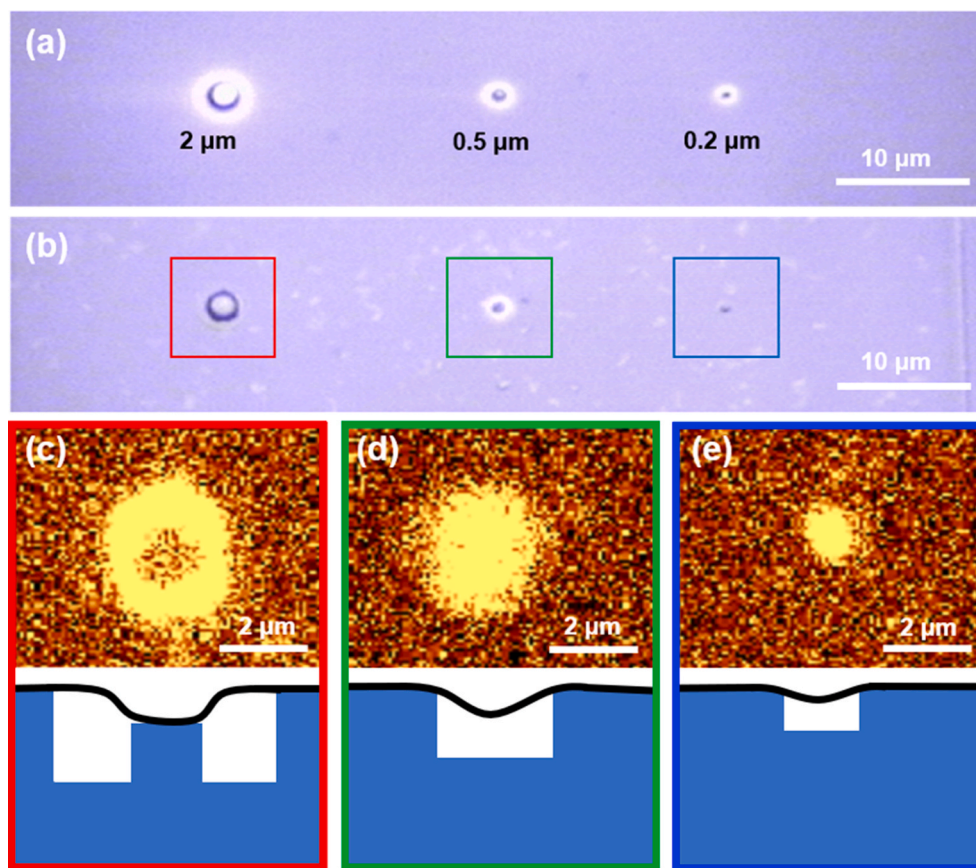


**Fig. 4.** (Color online) (a) An optical image of rings with different sizes made by FIB. (b) An optical image of the rings after graphene growth. (c)–(e) Raman mapping of 2D peak intensity of each ring indicated by rectangles drawn in the same color in (b). Insets in (c)–(e) are schematic side views of the freestanding graphene on the rings. (For interpretation of the references to color in this figure legend, the reader is referred to the Web version of this article.)

and line profiles were acquired using a CONTPT-10 probe with a resonance frequency of 13 kHz and a force constant of 0.2 N/m (NANO WORLD).

#### Declaration of competing interest

The authors declare that they have no known competing financial interests or personal relationships that could have appeared to influence the work reported in this paper.

#### Acknowledgments

This study was supported by a grant from the National Research Foundation of Korea (NRF-2019R1A2C1087494). SHW was supported by National Research Foundation of Korea (NRF) grant funded by the Korean Government (MEST) (2017R1E1A1A01074504).

The data that supports the findings of this study are available within the article.

#### References

- [1] W. Tappi JournalBao, G. Liu, Z. Zhao, H. Zhang, D. Yan, A. Deshpande, B. LeRoy, C. N. Lau, *Nano Res* 3 (2010) 98–102.
- [2] Z. Cheng, Q. Li, Z. Li, Q. Zhou, Y. Fang, *Nano Lett.* 10 (2010) 1864–1868.
- [3] J.C. Meyer, A.K. Geim, M.I. Katsnelson, K.S. Novoselov, D. Obergfell, S. Roth, C. Girit, A. Zettl, *Solid State Commun.* 143 (2007) 101–109.
- [4] J.-H. Park, D.-H. Cho, Y. Moon, H.-C. Shin, S.-J. Ahn, S.K. Kwak, H.-J. Shin, C. Lee, J.R. Ahn, *ACS Nano* 8 (2014) 11657–11665.
- [5] K.I. Bolotin, K. Sikes, Z. Jiang, M. Klima, G. Fudenberg, J. Hone, P. Kim, H. Stormer, *Solid State Commun.* 146 (2008) 351–355.
- [6] J.C. Meyer, A.K. Geim, M.I. Katsnelson, K.S. Novoselov, T.J. Booth, S. Roth, *Nature* 446 (2007) 60–63.
- [7] K. Bolotin, K. Sikes, J. Hone, H. Stormer, P. Kim, *Phys. Rev. Lett.* 101 (2008), 096802.
- [8] C. Martin-Olmos, H.I. Rasool, B.H. Weiller, J.K. Gimzewski, *ACS Nano* 7 (2013) 4164–4170.
- [9] B. Zhang, Q. Li, T. Cui, *Biosens. Bioelectron.* 31 (2012) 105–109.
- [10] C. Lee, X. Wei, J.W. Kysar, J. Hone, *Science* 321 (2008) 385–388.
- [11] C. Riedl, C. Coletti, T. Iwasaki, A.A. Zakharov, U. Starke, *Phys. Rev. Lett.* 103 (2009) 246804.
- [12] S.L. Wong, H. Huang, Y. Wang, L. Cao, D. Qi, I. Santos, W. Chen, A.T.S. Wee, *ACS Nano* 5 (2011) 7662–7668.
- [13] J.W. Suk, A. Kitt, C.W. Magnuson, Y. Hao, S. Ahmed, J. An, A.K. Swan, B. B. Goldberg, R.S. Ruoff, *ACS Nano* 5 (2011) 6916–6924.
- [14] W. Cai, A.L. Moore, Y. Zhu, X. Li, S. Chen, L. Shi, R.S. Ruoff, *Nano Lett.* 10 (2010) 1645–1651.
- [15] A. Smith, F. Niklaus, A. Paussa, S. Vaziri, A.C. Fischer, M. Sterner, F. Forsberg, A. Delin, D. Esseni, P. Palestri, *Nano Lett.* 13 (2013) 3237–3242.
- [16] S. Shivaraman, R.A. Barton, X. Yu, J. Alden, L. Herman, M.V.S. Chandrashekar, J. Park, P.L. McEuen, J.M. Parpia, H.G. Craighead, M.G. Spencer, *Nano Lett.* 9 (2009) 3100–3105.
- [17] H.W. Kim, H.W. Yoon, S.-M. Yoon, B.M. Yoo, B.K. Ahn, Y.H. Cho, H.J. Shin, H. Yang, U. Paik, S. Kwon, *Science* 342 (2013) 91–95.
- [18] L. Huang, M. Zhang, C. Li, G. Shi, *J. Phys. Chem. Lett.* 6 (2015) 2806–2815.
- [19] B.M. Venkatesan, R. Bashir, *Nat. Nanotechnol.* 6 (2011) 615–624.
- [20] G.F. Schneider, S.W. Kowalczyk, V.E. Calado, G. Pandraud, H.W. Zandbergen, L. M. Vandersypen, C. Dekker, *Nano Lett.* 10 (2010) 3163–3167.
- [21] C.A. Merchant, K. Healy, M. Wanunu, V. Ray, N. Peterman, J. Bartel, M. D. Fischbein, K. Venta, Z. Luo, A.C. Johnson, *Nano Lett.* 10 (2010) 2915–2921.
- [22] T. Miao, S. Yeom, P. Wang, B. Standley, M. Bockrath, *Nano Lett.* 14 (2014) 2982–2987.
- [23] Q. Wang, W. Hong, L. Dong, *Nanoscale* 8 (2016) 7663–7671.
- [24] P. Waduge, J. Larkin, M. Upmanyu, S. Kar, M. Wanunu, *Small* 11 (2015) 597–603.
- [25] K.S. Kim, Y. Zhao, H. Jang, S.Y. Lee, J.M. Kim, K.S. Kim, J.-H. Ahn, P. Kim, J.-Y. Choi, B.H. Hong, *Nature* 457 (2009) 706–710.
- [26] A.C. Ferrari, D.M. Basko, *Nat. Nanotechnol.* 8 (2013) 235–246.
- [27] Z. Ni, W. Chen, X. Fan, J. Kuo, T. Yu, A. Wee, Z. Shen, *Phys. Rev. B* 77 (2008) 115416.
- [28] J. Röhr, M. Hundhausen, K. Emtsev, T. Seyller, R. Graupner, L. Ley, *Appl. Phys. Lett.* 92 (2008) 201918.
- [29] N. Ferralis, R. Maboudian, C. Carraro, *Phys. Rev. Lett.* 101 (2008) 156801.

- [30] F. Fromm, M. Oliveira Jr., A. Molina-Sanchez, M. Hundhausen, J. Lopes, H. Riechert, L. Wirtz, T. Seyller, *New J. Phys.* 15 (2013), 043031.
- [31] J.A. Robinson, M. Wetherington, J.L. Tedesco, P.M. Campbell, X. Weng, J. Stitt, M. A. Fanton, E. Frantz, D. Snyder, B.L. VanMil, G.G. Jernigan, R.L. Myers-Ward, C. R. Eddy, D.K. Gaskill, *Nano Lett.* 9 (2009) 2873–2876.
- [32] D. Waldmann, J. Jobst, F. Speck, T. Seyller, M. Krieger, H.B. Weber, *Nat. Mater.* 10 (2011) 357–360.
- [33] J. Hannon, R. Tromp, *Phys. Rev. B* 77 (2008) 241404.
- [34] M. Hupalo, E. Conrad, M. Tringides, *Phys. Rev. B* 80 (2009), 041401.